ADVANCES IN ATMOSPHERIC SCIENCES, VOL. 27, NO. 4, 2010, 728–740

Application of the Characteristic CIP Method to a Shallow Water Model on the Sphere

PENG Xindong*[1] (彭新东), CHANG Yan[2] (常 燕), LI Xingliang[1] (李兴良), and XIAO Feng[3,4] (肖 锋)

[1]*State Key Laboratory of Severe Weather, Chinese Academy of Meteorological Sciences, Beijing* 100081

[2]*College of Atmospheric Sciences, Lanzhou University, Lanzhou* 730000

[3]*Institute of Mechanics, Chinese Academy of Sciences, Beijing* 100081

[4]*Tokyo Institute of Technology, Tokyo, Japan*

(Received 31 August 2009; revised 27 October 2009)

ABSTRACT

Semi-implicit algorithms are popularly used to deal with the gravitational term in numerical models. In this paper, we adopt the method of characteristics to compute the solutions for gravity waves on a sphere directly using a semi-Lagrangian advection scheme instead of the semi-implicit method in a shallow water model, to avoid expensive matrix inversions. Adoption of the semi-Lagrangian scheme renders the numerical model always stable for any Courant number, and which saves CPU time. To illustrate the efficiency of the characteristic constrained interpolation profile (CIP) method, some numerical results are shown for idealized test cases on a sphere in the Yin-Yang grid system.

Key words: characteristic CIP method, shallow-water model, Yin-Yang grid, semi-Lagrangian scheme, gravity wave

Citation: Peng, X. D., Y. Chang, X. L. Li, and F. Xiao, 2010: Application of the characteristic CIP method to a shallow water model on the sphere. *Adv. Atmos. Sci.*, **27**(4), 728–740, doi: 10.1007/s00376-009-9148-6.

1. Introduction

Computational efficiency and accuracy are two important characteristics in the field of computational fluid dynamics, and the notion of "the higher the better" seems to be true for numerical weather forecasting. To achieve better numerical properties, researchers have invented various finite deference schemes (Crowley, 1968; Tremback et al., 1987; Morinishi et al., 2004). Besides providing high-precision results, high-order schemes also have high costs (low computational efficiency). To address these tradeoffs, we must find a point of balance between the computational accuracy and cost. Many efforts have been made by researchers around the world to improve the computational efficiency and/or accuracy, such as the use of advanced temporal and spatial integration algorithms (e.g., Runge-Kutta method, semi-implicit, and semi-Lagrange methods, etc.). The high-order Runge-Kutta scheme (Gill, 1951) is much better in terms of stability, and can be used with a larger time step, than the Euler forward method. Being a multi-step scheme, however, it takes more computational resources for a single step of integration. The semi-Lagrangian scheme, which enlarges the time step for advection, is known as one of the most effective algorithms (Staniforth and Côté, 1991). Variations on this kind method (e.g., Yabe and Aoki, 1991; McGregor, 1996; Zerroukat et al., 2002) have been developed for effective computation, and are already used in atmospheric models. A successful application of the semi-implicit method for gravity waves which is stable successfully extends the computational time step. In computational geophysical fluid dynamics, the definition or selection of a proper grid system is known to be a useful way to cut cost and improve numerical representations (Rančić et al., 1996; McGregor, 1996; Kageyama and Sato, 2004). We tend to use uniform grid systems in numerical models because no severe restriction on the time step exists in concern with much

*Corresponding author: PENG Xindong, pengxd@cams.cma.gov.cn

smaller grid spacing. In more general geophysical fluid dynamics modeling, rigorous restrictions must be considered for all the dynamical processes, such as advection and wave propagation. Generally, a rapid wave is harder to deal with within these restrictions on speed vs. grid spacing than the flow because waves can travel so much faster.

Gravity waves, also known as fast waves, are dynamical processes that contribute to weather variation. Explicit and semi-implicit schemes have been developed to treat the gravity waves in numerical models. The explicit scheme is conditionally stable, and the time step is severely restricted by the top gravity wave speed. Even though the semi-implicit scheme is stable, a matrix inversion is not avoidable, which is expensive for high resolution cases and hard to parallelize. With the definition of a Riemann invariant, Ogata and Yabe (2004) solved the shallow water equation in a Cartesian coordinate system using the characteristic approach. In Ogata and Yabe (2004), the gravity wave is solved with the semi-Lagrangian method in addition to the advection, which renders the integration always stable and is free of expensive matrix computations in the model. In practical application, it is important to develop an algorithm for the characteristic method in spherical geometry. In this paper, we will first show the aforementioned algorithm, and then give the results of an application to a shallow water equation with topography on a sphere using the characteristic method.

The Constrained Interpolation Profile (CIP) method (Yabe and Aoki, 1991) has been widely used in computational fluid dynamics (Xiao et al., 1996; Yabe et al., 2001), and is also applied in atmospheric models (Peng et al., 2003; 2005). As a multi-moment semi-Lagrangian scheme (Xiao, 2004), CIP achieves high accuracy with relatively less stencils. For the spherical shallow water equations, Peng et al. (2006) developed a conservative constraint for the overlapped Yin-Yang grid, and tested this with idealized advection cases. It shows the successful application of the CIP scheme on the Yin-Yang grid, and has good numerical properties.

In this paper, we also employ the CIP scheme to solve the shallow water equations with the so-called characteristic method on the Yin-Yang grid. The characteristic algorithm on a sphere will be presented in section 2. The numerical schemes used in this paper and the computational procedure will appear in section 3. A brief introduction to the test cases is provided in section 4, and the corresponding results will be illustrated in section 5. Finally, concluding remarks are presented in section 6.

2. Characteristic method for shallow water equation on sphere

The characteristic method was first proposed in detail by Rusanov (1963) for use in the context of gas dynamics. These kinds of schemes treat the nonlinear wave propagation in direct relationship to the rest of the fluid dynamics. The basic idea is to compute the nonlinear effect of various waves with the help of the Riemann invariant. Generally, multi-dimensional problems are approached with dimensional splitting, and the waves travel independently along the coordinate axes. In the field of the gas dynamics, Cartesian coordinates are well used for application of the characteristic method.

For the case of a geophysical shallow water model, the equations are solved in spherical geometry. We present the two-dimensional algorithm for Riemann problems on a sphere in the appearance of mean flow and gravity waves in this section. A non-conservative algorithm is adopted here by using advection-type equations. The shallow water equations on a sphere can be written as follows:

$$\begin{cases} \dfrac{\partial h^*}{\partial t} + \boldsymbol{V}\cdot\nabla h^* + \dfrac{h^*}{a\cos\varphi}\left(\dfrac{\partial u}{\partial\lambda} + \dfrac{\partial v\cos\varphi}{\partial\varphi}\right) = 0\,, \\ \dfrac{\partial u}{\partial t} + \boldsymbol{V}\cdot\nabla u - \left(f + \dfrac{u}{a}\tan\varphi\right)v + \dfrac{g}{a\cos\varphi}\dfrac{\partial h}{\partial\lambda} = 0\,, \\ \dfrac{\partial v}{\partial t} + \boldsymbol{V}\cdot\nabla v + \left(f + \dfrac{u}{a}\tan\varphi\right)u + \dfrac{g}{a}\dfrac{\partial h}{\partial\varphi} = 0\,, \end{cases} \tag{1}$$

and

$$h = h^* + h_{\mathrm{s}}\,,$$

where h^* is the depth of the fluid, and h_{s} is the topography. The variable h is the height of the fluid surface. The latitude and longitude are φ and λ; f and g are the Coriolis parameter and the gravitational constant, respectively. The horizontal wind components are u and v, and the horizontal wind vector is $\boldsymbol{V} = (u, v)$.

The Eq. (1) can be rewritten as

$$\begin{cases} \dfrac{\partial h^*}{\partial t} + \dfrac{1}{a\cos\varphi}\left(u\dfrac{\partial h^*}{\partial\lambda} + h^*\dfrac{\partial u}{\partial\lambda}\right) + \\ \dfrac{1}{a}\left(v\dfrac{\partial h^*}{\partial\varphi} + h\dfrac{\partial v}{\partial\varphi}\right) - \dfrac{h^* v}{a}\tan\varphi = 0\,, \\ \dfrac{\partial u}{\partial t} + \dfrac{1}{a\cos\varphi}\left(u\dfrac{\partial u}{\partial\lambda} + g\dfrac{\partial h^*}{\partial\lambda}\right) + \dfrac{1}{a}v\dfrac{\partial u}{\partial\varphi} - \\ \left(f + \dfrac{u}{a}\tan\varphi\right)v + \dfrac{g}{a\cos\varphi}\dfrac{\partial h_{\mathrm{s}}}{\partial\lambda} = 0\,, \\ \dfrac{\partial v}{\partial t} + \dfrac{1}{a\cos\varphi}u\dfrac{\partial v}{\partial\lambda} + \dfrac{1}{a}\left(v\dfrac{\partial v}{\partial\varphi} + g\dfrac{\partial h^*}{\partial\varphi}\right) + \\ \left(f + \dfrac{u}{a}\tan\varphi\right)u + \dfrac{g}{a}\dfrac{\partial h_{\mathrm{s}}}{\partial\varphi} = 0\,. \end{cases} \tag{2}$$

Let

$$\boldsymbol{W} = \begin{bmatrix} h^* \\ u \\ v \end{bmatrix} ,$$

and then the Eq. (2) can be further written in vector form as

$$\frac{\partial \boldsymbol{W}}{\partial t} + \boldsymbol{P}\frac{\partial \boldsymbol{W}}{\partial \lambda} + \boldsymbol{Q}\frac{\partial \boldsymbol{W}}{\partial \varphi} + \boldsymbol{F} = 0 , \tag{3}$$

where the matrices are

$$\boldsymbol{P} = \frac{1}{a\cos\varphi}\begin{bmatrix} u & h^* & 0 \\ g & u & 0 \\ 0 & 0 & u \end{bmatrix} ,$$

$$\boldsymbol{Q} = \frac{1}{a}\begin{bmatrix} v & 0 & h^* \\ 0 & v & 0 \\ g & 0 & v \end{bmatrix}$$

and the forcing term is

$$\boldsymbol{F} = \begin{bmatrix} -\dfrac{h^* v}{a}\tan\varphi \\ -\left(f + \dfrac{u}{a}\tan\varphi\right) v + \dfrac{g}{a\cos\varphi}\dfrac{\partial h_\mathrm{s}}{\partial \lambda} \\ \left(f + \dfrac{u}{a}\tan\varphi\right) u + \dfrac{g}{a}\dfrac{\partial h_\mathrm{s}}{\partial \varphi} \end{bmatrix} .$$

Under the basic philosophy of solving the nonlinear Eq. (3) with a dimensional splitting procedure, the solution can be approached by solving

$$\frac{\partial \boldsymbol{W}}{\partial t} + \boldsymbol{F} = 0 , \tag{4}$$

$$\frac{\partial \boldsymbol{W}}{\partial t} + \boldsymbol{P}\frac{\partial \boldsymbol{W}}{\partial \lambda} = 0 , \tag{5}$$

$$\frac{\partial \boldsymbol{W}}{\partial t} + \boldsymbol{Q}\frac{\partial \boldsymbol{W}}{\partial \varphi} = 0 , \tag{6}$$

sequentially. It is easy to find that Eq. (4) describes the forcing term, and Eqs. (5) and (6) are similar to the advection equation, which needs further transformation.

As an important step to solve Eqs. (5) and (6), the matrixes $\boldsymbol{P}$ and $\boldsymbol{Q}$ must be treated properly in order to obtain the temporal integration of $\boldsymbol{W}$. Firstly, we take Eq. (5) as the example to show the procedure. Given $\boldsymbol{P}$, we can get its eigenvalues by solving

$$|\boldsymbol{P} - \Lambda_\lambda \boldsymbol{I}| = 0 , \tag{7}$$

where $\boldsymbol{I}$ is an unit matrix. The solutions are

$$\Lambda_{\lambda,1,2} = \frac{1}{a\cos\varphi}(u \pm \sqrt{gh^*}) , \qquad \Lambda_{\lambda,3} = \frac{1}{a\cos\varphi}u . \tag{8}$$

Substituting these eigenvalues into the equation

$$\boldsymbol{P} - \Lambda_\lambda \boldsymbol{I} = 0 ,$$

the corresponding characteristic vectors for the three eigenvalues are obtained straightforwardly. These eigenvectors are

$$\boldsymbol{K}_1 = \begin{bmatrix} 1 \\ \sqrt{\dfrac{g}{h^*}} \\ 0 \end{bmatrix} , \quad \boldsymbol{K}_2 = \begin{bmatrix} 1 \\ -\sqrt{\dfrac{g}{h^*}} \\ 0 \end{bmatrix} , \quad \boldsymbol{K}_3 = \begin{bmatrix} 0 \\ 0 \\ 1 \end{bmatrix} . \tag{9}$$

The characteristic matrix, which is made up of the characteristic vectors, is therefore

$$\boldsymbol{E} = \begin{bmatrix} 1 & 1 & 0 \\ \sqrt{\dfrac{g}{h^*}} & -\sqrt{\dfrac{g}{h^*}} & 0 \\ 0 & 0 & 1 \end{bmatrix} , \tag{10}$$

and the inverse of this matrix is

$$\boldsymbol{E}^{-1} = \begin{bmatrix} \dfrac{1}{2} & \dfrac{1}{2}\sqrt{\dfrac{h^*}{g}} & 0 \\ \dfrac{1}{2} & -\dfrac{1}{2}\sqrt{\dfrac{h^*}{g}} & 0 \\ 0 & 0 & 1 \end{bmatrix} . \tag{11}$$

The relationship between the eigenvalues and characteristic matrix is

$$\boldsymbol{E}^{-1}\boldsymbol{P}\boldsymbol{E} = \begin{bmatrix} \Lambda_{\lambda,1} & 0 & 0 \\ 0 & \Lambda_{\lambda,2} & 0 \\ 0 & 0 & \Lambda_{\lambda,3} \end{bmatrix} .$$

Equation (5) can be expressed as

$$\boldsymbol{E}^{-1}\frac{\partial \boldsymbol{W}}{\partial t} + \boldsymbol{E}^{-1}\boldsymbol{P}\frac{\partial \boldsymbol{W}}{\partial \lambda} = 0 ,$$

if multiplied with $\boldsymbol{E}^{-1}$. Considering

$$\boldsymbol{E}^{-1}\boldsymbol{P} = \boldsymbol{E}^{-1}\boldsymbol{P}\boldsymbol{E}\boldsymbol{E}^{-1} = \begin{bmatrix} \Lambda_{\lambda,1} & 0 & 0 \\ 0 & \Lambda_{\lambda,2} & 0 \\ 0 & 0 & \Lambda_{\lambda,3} \end{bmatrix} \boldsymbol{E}^{-1} ,$$

further transformation of the equation leads

$$\boldsymbol{E}^{-1}\frac{\partial \boldsymbol{W}}{\partial t} + \begin{bmatrix} \Lambda_{\lambda,1} & 0 & 0 \\ 0 & \Lambda_{\lambda,2} & 0 \\ 0 & 0 & \Lambda_{\lambda,3} \end{bmatrix} \boldsymbol{E}^{-1}\frac{\partial \boldsymbol{W}}{\partial \lambda} = 0 , \tag{12}$$

which is equivalent to Eq. (5). Expansion of Eq. (12) gives

$$\begin{cases} \dfrac{\partial\left(\Gamma+\dfrac{u}{2}\right)}{\partial t}+\Lambda_{\lambda,1}\dfrac{\partial\left(\Gamma+\dfrac{u}{2}\right)}{\partial\lambda}=0\,, \\ \dfrac{\partial\left(\Gamma-\dfrac{u}{2}\right)}{\partial t}+\Lambda_{\lambda,2}\dfrac{\partial\left(\Gamma-\dfrac{u}{2}\right)}{\partial\lambda}=0\,, \\ \dfrac{\partial v}{\partial t}+\Lambda_{\lambda,3}\dfrac{\partial v}{\partial\lambda}=0\,, \end{cases} \tag{13}$$

and $\Gamma=\sqrt{gh^*}$ is the speed of gravity waves. Equation (13) is obviously in their typical advective forms, which can be solved numerically with the CIP (Yabe and Aoki, 1991) scheme. The Riemann invariants, $\Gamma\pm u/2$ and v, are transported by the eigenvalues, respectively. It is interesting that $\Lambda_{\lambda,1,2}$ shows the combination of the horizontal velocity and the propagation of the gravity wave. Equation (13) shows the intrinsic relationship between the fluid depth and the flow in the dynamical sense. The Riemann invariants are exactly transported by the universal velocity that is known as an integral of the basic flow wind and the gravity wave solution.

Similarly, the advection equations in the φ direction are given by:

$$\begin{cases} \dfrac{\partial\left(\Gamma+\dfrac{v}{2}\right)}{\partial t}+\Lambda_{\varphi,1}\dfrac{\partial\left(\Gamma+\dfrac{v}{2}\right)}{\partial\varphi}=0\,, \\ \dfrac{\partial\left(\Gamma-\dfrac{v}{2}\right)}{\partial t}+\Lambda_{\varphi,2}\dfrac{\partial\left(\Gamma-\dfrac{v}{2}\right)}{\partial\varphi}=0\,, \\ \dfrac{\partial u}{\partial t}+\Lambda_{\varphi,3}\dfrac{\partial u}{\partial\varphi}=0\,. \end{cases} \tag{14}$$

The eigenvalues are represented as

$$\begin{cases} \Lambda_{\varphi,1}=\left(v+\sqrt{gh^*}\right)\Big/a\,, \\ \Lambda_{\varphi,2}=\left(v-\sqrt{gh^*}\right)\Big/a\,, \\ \Lambda_{\varphi,3}=v/a\,. \end{cases} \tag{15}$$

The three in Eq. (14) can be integrated with the CIP scheme in the same way as in the λ direction, so that a large time step is possible. The advection velocity is found to be the summation of wind and wave speeds.

Besides Eqs. (5) and (6), Eq. (4) must also be solved in a proper way so that the total computational efficiency is not influenced negatively. Equation (4) describes the forcing terms due to the Coriolis force and topography, and it can be computed semi-implicitly. The details will be shown in the next section.

3. Numerical schemes and computational procedure

3.1 *Brief description of the advection scheme for CIP and the boundary condition arrangement*

By introducing the characteristic method, the spherical shallow water model is divided into three parts. The first two parts are found to be typical advection problem of the Riemann invariant, and the third part is related to the forcing terms. For the advection Eqs. (13) and (14), the CIP method (Yabe and Aoki, 1991) is a robust scheme of high accuracy, even though it gives a non-conservative solution. Similar to Peng et al. (2003), the fluid depth and horizontal wind components can be computed with splitting techniques. Therefore, a one-dimensional CIP algorithm will be adopted to treat the λ- and φ-direction transports, which is preferable to third-order accuracy.

In the CIP scheme, two moments, namely the advection variable and its spatial derivative, are defined. In the present study, we will need to define h, u, v and the corresponding spatial gradients h_λ, h_φ, u_λ, u_φ, v_λ, v_φ at each of the grid-points of the two-dimensional domain. The subscript λ and φ shows the gradient in that direction. Please refer to Yabe and Aoki (1991) for more details of the one-dimensional CIP scheme.

In the Yin-Yang grid system, boundary conditions must be specified by interpolation or conservative constraints. The scalar variables can be interpolated directly, and the vectors are transformed in a different coordinate system after the interpolation. In the CIP scheme, derivatives, in addition to the physical variables, are used to construct the interpolation polynomials. The boundary conditions of the horizontal gradients of a scalar variable (e.g., h_λ, h_φ) can be arranged in the same way as for vectors, but it will be much more complex to arrange the derivatives of a vector (e.g., u_λ, u_φ, v_λ and v_φ) at a boundary. Subscripts "O" denoting the original zone, and "T" denoting the target system (i.e., Yin or Yang) are used to show how the gradient transformation between Yin and Yang is made:

$$\begin{bmatrix} \dfrac{\partial u}{\partial \lambda} \\ \dfrac{\partial v}{\partial \lambda} \\ \dfrac{\partial u}{\partial \varphi} \\ \dfrac{\partial v}{\partial \varphi} \end{bmatrix}_{\mathrm{T}} =$$

$$\frac{y_{\mathrm{O}}^2 z_{\mathrm{O}}^2}{R_{\mathrm{T}}^2 R_{\mathrm{O}}^2} \begin{bmatrix} \dfrac{R_{\mathrm{T}}}{R_{\mathrm{O}}} & \alpha\dfrac{R_{\mathrm{T}}}{R_{\mathrm{O}}} & \alpha R_{\mathrm{T}} & \alpha^2 R_{\mathrm{T}} \\ -\alpha\dfrac{R_{\mathrm{T}}}{R_{\mathrm{O}}} & \dfrac{R_{\mathrm{T}}}{R_{\mathrm{O}}} & -\alpha^2 R_{\mathrm{T}} & \alpha R_{\mathrm{T}} \\ -\alpha\dfrac{1}{R_{\mathrm{O}}} & -\alpha^2\dfrac{1}{R_{\mathrm{O}}} & 1 & \alpha \\ \alpha^2\dfrac{1}{R_{\mathrm{O}}} & -\alpha\dfrac{1}{R_{\mathrm{O}}} & -\alpha & 1 \end{bmatrix} \begin{bmatrix} \dfrac{\partial u}{\partial \lambda} \\ \dfrac{\partial v}{\partial \lambda} \\ \dfrac{\partial u}{\partial \varphi} \\ \dfrac{\partial v}{\partial \varphi} \end{bmatrix}_{\mathrm{O}} +$$

$$\frac{1}{R_{\mathrm{T}}^2 R_{\mathrm{O}}^3} \begin{bmatrix} R_{\mathrm{T}} x_{\mathrm{O}} y_{\mathrm{O}} & -R_{\mathrm{T}} y_{\mathrm{O}}^2 z_{\mathrm{O}} \\ R_{\mathrm{T}} y_{\mathrm{O}}^2 z_{\mathrm{O}} & R_{\mathrm{T}} x_{\mathrm{O}} y_{\mathrm{O}} \\ -x_{\mathrm{O}}^2 z_{\mathrm{O}} & x_{\mathrm{O}} y_{\mathrm{O}} z_{\mathrm{O}}^2 \\ -x_{\mathrm{O}} y_{\mathrm{O}} z_{\mathrm{O}}^2 & -x_{\mathrm{O}}^2 z_{\mathrm{O}} \end{bmatrix} \begin{bmatrix} u \\ v \end{bmatrix}_{\mathrm{O}}, \tag{16}$$

where $R = \cos\varphi$ and

$$\alpha = \frac{x_{\mathrm{o}}}{y_{\mathrm{o}} z_{\mathrm{o}}}$$

are defined, and x, y, and z are the three-dimensional coordinates, respectively. The boundary condition for a scalar and any component of the vectors can be interpolated using high-order polynomials before the transformation.

3.2 *Semi-implicit computation of inertial forces*

In a spherical shallow water equation system, gravity and inertial waves exist. Integration of Eqs. (5) and (6) is stable for large Courant number with the aid of semi-Lagrangian computation. The inertial mode in Eq. (4), however, restricts the computational stability, as well. A semi-implicit scheme is then developed for the inertial term in Eq. (4) so as to enlarge the time-step. Considering the λ-direction forcing term, we show the semi-implicit integration of Eq. (4) as,

$$\begin{cases} u^* \pm 2\Gamma^* = \\ u_{\lambda_\pm} \pm 2\Gamma_{\lambda_\pm} + \dfrac{1}{2}\left\{\dfrac{1}{2}\left[fv^* + fv_{\lambda_\pm} + \right.\right. \\ \left.\left.\dfrac{\tan\varphi}{a}(u^* v^* + u_{\lambda_\pm} v_{\lambda_\pm})\right]\Delta t\right\}, \\ v^* = \\ v_{\lambda_0} - \dfrac{\Delta t}{4}\left[fu^* + fu_{\lambda_0} + \dfrac{\tan\varphi}{a}\times \right. \\ \left.(u^* u^* + u_{\lambda_0} u_{\lambda_0})\right], \end{cases} \tag{17}$$

where the superscript $*$ denotes the final value that counts the forcing term, and the subscripts $\lambda_\pm$ and λ_0 represent the variables after advection by computation with Eq. (13). The forcing terms in Eq. (4) is divided into two parts, which are computed separately in the λ direction with Eq. (17) and the φ direction, so that they are symmetrically computed in the splitting procedure. The relevant solution can be calculated as:

$$\begin{aligned} \Gamma^* = \Big\{ & u_{\lambda_+} - u_{\lambda_-} + 2(\Gamma_{\lambda_+} + \Gamma_{\lambda_-}) + \\ & \frac{\Delta t}{4}\left[\left(f + \frac{\tan\varphi}{a} u_{\lambda_+}\right) v_{\lambda_+} - \right. \\ & \left.\left(f + \frac{\tan\varphi}{a} u_{\lambda_-}\right) v_{\lambda_-}\right]\Big\}/4, \end{aligned} \tag{18}$$

$$u^* = -\frac{B}{3A} - \frac{2^{1/3}(-B^2 + 3AC)}{3A[-2B^3 + 9ABC - 27A^2 D + \sqrt{4(-B^2 + 3AC)^3 + (-2B^3 + 9ABC - 27A^2 D)^2}]^{1/3}} + \frac{[-2B^3 + 9ABC - 27A^2 D + \sqrt{4(-B^2 + 3AC)^3 + (-2B^3 + 9ABC - 27A^2 D)^2}]^{1/3}}{3^* 2^{1/3} A}, \tag{19}$$

and

$$v^* = v_{\lambda_0} - \frac{\Delta t}{4}\left[\left(f + \frac{\tan\varphi}{a} u^*\right) u^* + \left(f + \frac{\tan\varphi}{a} u_{\lambda_0}\right) u_{\lambda_0}\right], \tag{20}$$

$$A = \left(\frac{\Delta t}{4}\frac{\tan\varphi}{a}\right)^2,$$

$$B = 2f\frac{\tan\varphi}{a}\left(\frac{\Delta t}{4}\right)^2,$$

where

$$C = 1 + \left(\frac{f\Delta t}{4}\right)^2 - \frac{\Delta t}{4}\frac{\tan\varphi}{a}v_{\lambda_0} + \left(\frac{\Delta t}{4}\right)^2 \frac{\tan\varphi}{a}\left(f + \frac{\tan\varphi}{a}u_{\lambda_0}\right)u_{\lambda_0} ,$$

$$D = -\frac{1}{2}(u_{\lambda+} + u_{\lambda-}) - (\Gamma_{\lambda+} + \Gamma_{\lambda-}) - \frac{f\Delta t}{4}v_{\lambda_0} + f\left(\frac{\Delta t}{4}\right)^2\left(f + \frac{\tan\varphi}{a}u_{\lambda_0}\right)u_{\lambda_0} - \frac{\Delta t}{8}\left[\left(f + \frac{\tan\varphi}{a}u_{\lambda+}\right)v_{\lambda+} + \left(f + \frac{\tan\varphi}{a}u_{\lambda-}\right)v_{\lambda-}\right] .$$

The semi-implicit solution is represented in Eqs. (18)–(20) by considering the forcing term and advection in the λ-direction, and the semi-implicit formula in the φ-direction can be written in a similar way as:

$$v^* \pm 2\Gamma^* = v_{\varphi\pm} \pm 2\Gamma_{\varphi\pm} - \frac{1}{2}\left\{\frac{1}{2}\left[fu^* + fu_{\varphi\pm} + \frac{\tan\varphi}{a}(u^*u^* + u_{\varphi\pm}u_{\varphi\pm})\right]\Delta t\right\} ,$$

$$u^* = u_{\varphi_0} + \frac{1}{2}\left\{\frac{1}{2}\left[fv^* + fv_{\varphi_0} + \frac{\tan\varphi}{a}(u^*v^* + u_{\varphi_0}v_{\varphi_0})\right]\Delta t\right\} . \quad (21)$$

The analytical solution is:

$$\Gamma^* = \frac{1}{4}\left\{v_{\varphi+} - v_{\varphi-} + 2(\Gamma_{\varphi+} + \Gamma_{\varphi-}) - \frac{\Delta t}{4}\left[\left(f + \frac{\tan\varphi}{a}u_{\varphi+}\right)u_{\varphi+} - \left(f + \frac{\tan\varphi}{a}u_{\varphi-}\right)u_{\varphi-}\right]\right\} , \quad (22)$$

and u^* shows the same expression as in Eq. (19) but with

$$A = \left(\frac{\Delta t}{4}\frac{\tan\varphi}{a}\right)^2 ,$$

$$B = 2f\frac{\tan\varphi}{a}\left(\frac{\Delta t}{4}\right)^2 ,$$

$$C = 1 - \frac{\Delta t}{8}\left(\frac{\tan\varphi}{a}\xi - \frac{\Delta t}{2}f^2\right) ,$$

$$D = -u_{\varphi_0} + \frac{\Delta t}{4}\left(f + \frac{\tan\varphi}{a}u_{\varphi_0}\right)v_{\varphi_0} - \frac{\Delta t}{8}f\xi ,$$

where

$$\xi = v_{\varphi+} + v_{\varphi-} + 2(\Gamma_{\varphi+} - \Gamma_{\varphi-}) - \frac{\Delta t}{4}\frac{\tan\varphi}{a}[(u_{\varphi+})^2 + (u_{\varphi-})^2] - \frac{\Delta t}{4}f(u_{\varphi+} + u_{\varphi-}) .$$

The v^* component is calculated as

$$v^* = \frac{1}{2}[v_{\varphi+} + v_{\varphi-} + 2(\Gamma_{\varphi+} - \Gamma_{\varphi-})] - \frac{\Delta t}{8}\left[\frac{2\tan\varphi}{a}u^{*2} + 2fu^* + f(u_{\varphi+} + u_{\varphi-}) + \frac{\tan\varphi}{a}(u_{\varphi+}u_{\varphi+} + u_{\varphi-}u_{\varphi-})\right] . \quad (23)$$

Despite of the complexity of Eq. (23), the computations involved are very cost effective because of its exact analytical nature. There is no need to solve any Poisson equation and matrix problem, even though the Coriolis term is treated semi-implicitly.

The computational procedure can be summarized briefly as follows. First, compute the "advection" by the dimensional splitting method following Eqs. (13) and (14) using the CIP scheme. The wind components (u, v) and the geopotential height (h^*) are transported consequently in the spatial directions. Second, the equations take account of the forcing terms, including the Coriolis term, semi-implicitly according to Eqs. (17) and (21). In this step, the calculation is also conducted with a dimensional splitting method. Finally, the remaining forcing terms of Eq. (4) are accounted for. The topographic terms of $\partial h_s/\partial\lambda$ and $\partial h_s/\partial\varphi$ can be computed with a central difference method. In the idealized test cases (section 5), we use the analytical solution. The result is

$$\begin{bmatrix} u^* \\ v^* \end{bmatrix}_{n+1} = \begin{bmatrix} u^* - \dfrac{g}{a\cos\varphi}\dfrac{\partial h_s}{\partial\lambda}\Delta t \\ v^* - \dfrac{g}{a}\dfrac{\partial h_s}{\partial\varphi}\Delta t \end{bmatrix} .$$

The forcing term of h^* is also computed semi-implicitly as:

$$h^*_{n+1} = h^*\frac{1 + \Delta t v^*\tan\varphi/2a}{1 - \Delta t v^*\tan\varphi/2a} .$$

The subscript $n+1$ denotes the new time step, and $h^* = \Gamma^{*2}/g$.

4. Brief description of test cases

To evaluate the performance of the method and its treatment of gravity waves, test cases for the global shallow-water equation set on sphere from Williamson et al. (1992) are selected for practical computation in this study. The global steady state nonlinear zonal

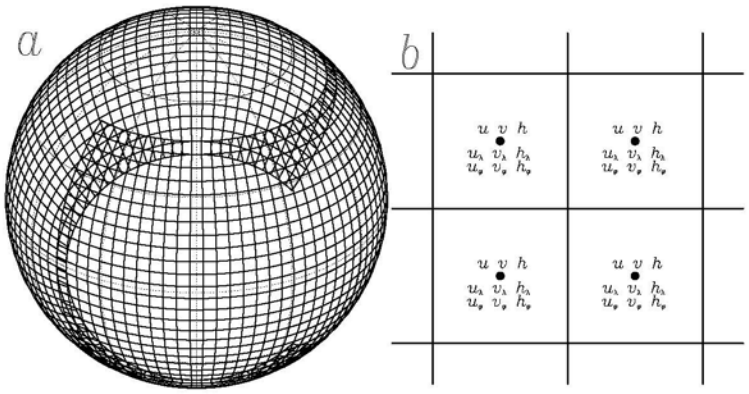

Fig. 1. Schematic illustration of (a) the Yin-Yang grid and (b) variable distribution in a cell in the shallow-water model. Variable u_λ, u_φ in (b) shows the derivative of u in λ direction andφ direction, respectively; and $v_\lambda, v_\varphi, h_\lambda, h_\varphi$ is similar.

geostrophic flow (case 2) and zonal flow over an isolated mountain (case 5) are tested in the shallow-water model. The results will be shown in the following section.

Test case 2 is a balanced geostrophic flow, which consists of zonal flow with the corresponding geostrophic height. The error norms can be estimated in comparison with the initial state. This provides a quantitative description of the numerical method and results. Case 5, however, is more complex, and lacks exact solutions. High-resolution model results can be used as a reference to illustrate the numerical accuracy of the CIP scheme by comparison. The detailed description of the test cases can be found in Williamson et al. (1992).

5. Configuration and numerical results for the shallow water equations

The Yin-Yang grid (Kageyama and Sato, 2004) is employed to discretize the shallow-water model. There is no pole in this grid system because of the globe is being composed of two zones that are cut from the lower-latitude region (usually 45°S–45°N in latitude and 45°W–45°E in longitude, see Fig. 1a). The grid spacing is quasi-uniform in each zone. The usual convergence of the longitude lines at high latitudes disappears from the system, therefore. One more merit of the grid system is the symmetric structure of the two zones. This allows the shallow water models on both zones to share the same code.

The cell number shows a proportion of 3:1 in the longitudinal and latitudinal directions. The resolution can be simply described with the latitudinal cell number (jp). To avoid a vector being located at the poles, the cell center, where all variables are defined (Fig. 1b), must not be located on the equator. The node point in Fig. 1b, on the other hand, is found at the south/north poles as well as at the equator.

A bi-fifth-order interpolation scheme is employed for the arrangement of the boundary conditions. As illustrated in Peng et al. (2006), additional constraints are needed to ensure global mass conservation in the Yin-Yang grid system. The characteristic method mentioned in this paper, however, makes use of the advection-form equation of the shallow-water model. No local conservation is considered in the present CIP scheme within a mesh cell. The conservation constraint that is developed in Peng et al. (2006) cannot be directly implemented into the present scheme, because no fluxes are available on cell boundaries. We then develop another simple modifier to ensure global mass conservation every time step. The basic consideration is to calculate the integral of mass (i.e., $I[h^*(\lambda,\varphi,t)]$) and the increment against the initial one (i.e., $\Re = I[h^*(\lambda,\varphi,t)] - I[h^*(\lambda,\varphi,0)]$). The modifier is given as

$$h^*_{\rm m}(\lambda,\phi,t) = h^*(\lambda,\phi,t)\,(1-\Re/I[h^*(\lambda,\phi,t)])\ , \quad (24)$$

where $h^*_{\rm m}(\lambda,\phi,t)$ denotes the modified value of $h^*(\lambda,\varphi,t)$, and $h^*(\lambda,\phi,t)|_{t=(n+1)\Delta t} = h^*_{n+1}$.

5.1 *Numerical result of Williamson et al.* (1992) *test case* 2

The test case of a steady geostrophic flow is carried out by using the characteristic method shown in section 3. A low resolution test with $jp = 34$ ($\Delta\lambda = \Delta\varphi = 2.90323$) is used here. The Courant-Friedrichs-Lewy (CFL) number is firstly taken to be 0.5, with a time step interval of 548 s in this case.

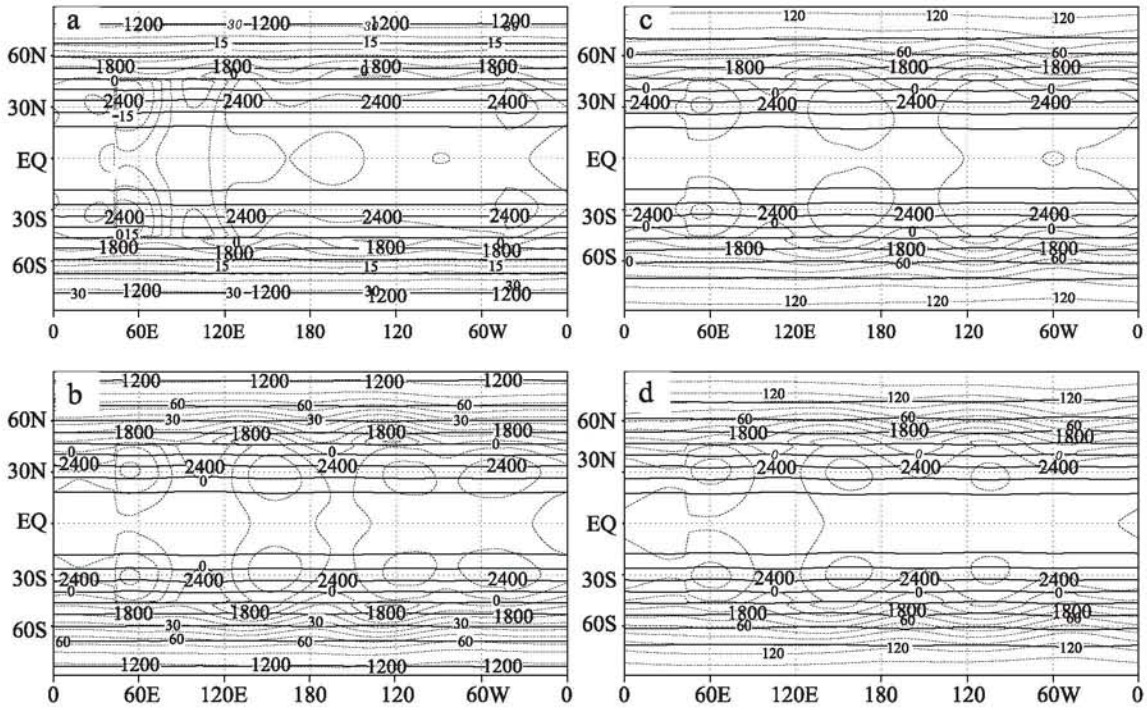

Fig. 2. Geopotential height (solid) and the corresponding absolute errors (dashed) at 3 (a), 7 (b), 10 (c) and 12 (d) days of the steady geostrophic flow.

Because the major objective is to evaluate the characteristic method in dealing with the gravity waves, $\alpha = 0$ is assumed in this case. The flow pattern in the Yang-grid zone is the same as that in the ordinary latitude-longitude coordinate system. In the Yin-grid zone, however, the wind does not flow along the line of latitude because it is normal to the Yang zone. Two vortexes appear on the poles, respectively. This pattern proves to be difficult to compute accurately. The feature makes it unnecessary to change the direction of the geostrophic flow for scheme evaluation.

A 12-day integration of the shallow-water model is executed on a Linux PC. In Fig. 2, the geopotential height (h) is plotted in comparison with its absolute error at 3, 7, 10, and 12 days. The steady distribution of geopotential height, which is shown to be parallel to lines of latitude, is simulated with reasonable accordance to the true solution. Little deformation is observed in the 12-day simulation in the Yang zone, though numerical diffusion is displayed in pole areas of the Yin zone. As a result, a generally realistic distribution is shown in this experiment with plausible parallel contours. The absolute error, however, displays more numerical bias at the up-stream boundary of the Yang-grid zone and in both pole regions. The former is clearly due the definition of the departure point, which is located in another zone (i.e., the Yin grid). As mentioned above, the flow pattern in the Yin-grid zone makes the calculation of the departure point much more inaccurate than in Yang zone. This is clearly due to the vector being uniform in each dimension of the Yang zone, but non-uniform in the Yin grid in this test case. Large errors result in high latitude region as a result of the pole points being located on the center of the environmental circumfluence in the Yin zone. Sharp variations of wind direction between neighboring points is indicated in both the latitudinal and longitudinal directions, which makes it hard to achieve perfect tracking of the departure point. Errors of departure point tracking are certainly increased in comparison with the uniform flow in the Yang zone.

Figure 3 displays the time series of L_2 and L_∞ norms (the same as defined in Peng et al., 2006) on the sphere. Both error norms increase linearly with time. As shown in Fig. 2, the norms are mainly the contribution of the numerical error in the Yin zone and in the adjacent Yang-zone border area. At day 12, L_2 and L_∞ have values of 0.019 and 0.05, respectively. The result displays the reasonability of the characteristic method developed here on the sphere in terms of accuracy. It still has potential to be used in large Courant number cases (and without matrix inversion). It is worth noting that the numerical errors become much larger if no modifications for global conservation are imposed. The errors make the geopotential height of the balanced flow become diffusive and contorted. This reveals the importance of conservation in the application of the characteristic method. Unfortunately,

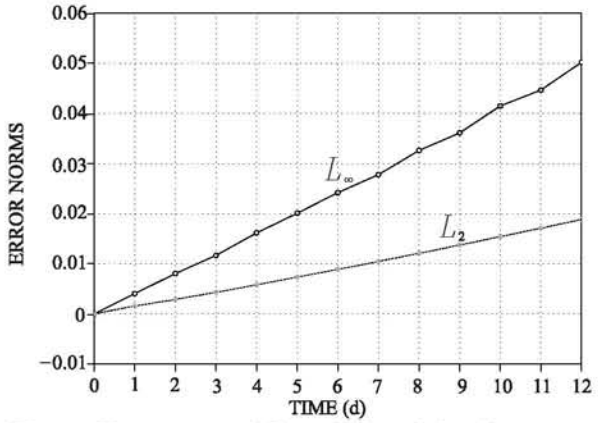

Fig. 3. Error norms of L_2 and L_∞ of the characteristic method with $jp = 34$ and CFL= 0.5.

the present scheme cannot make use of cell-boundary fluxes, and therefore no local conservation is ensured. In addition, the flow in the Yin zone is shown to be non-uniform in both directions, which is different from the original definition in the latitude-longitude coordinates. The dimensional convergence is applied for concern about avoiding numerical oscillations in a time splitting scheme. This is why we observe more errors in the Yin zone.

The primary motivation of developing the characteristic method on a sphere is to enlarge the integration time step in a dynamical model that does not require matrix inversion. The results above have shown the success of this method in the case of small Courant number conditions. To verify the ability to handle large Courant number cases, relatively high-resolution experiments with a configuration of $jp = 136$ are carried out under conditions of CFL numbers of 1.0, 1.5, 2.0, and 4.0. All experiments illustrate clearly the high stability and high computational performance of the method. Figure 4a shows the 2D geopotential height and absolute error at day 12 in case of CFL=1.5. Stable computation and a reasonable distribution of geopotential height reveal that the semi-Lagrangian treatment of gravity waves is capable of enlarging the usable time steps in a high-resolution model. Of course, more errors are inevitably displayed in comparison with the small CFL number case. If large Courant number is used with low-resolution cases (e.g., $jp = 34$), numerical noise increases obviously in the adjacent boundary areas to the Yang zone and in the whole Yin grid. This shortcoming is not a necessary result of using the method, because the characteristic method is developed for fine-mesh models when the matrix inversion has become too expensive in a semi-implicit semi-Lagrangian model. In a high-resolution model, there is still space left to enlarge time step (e.g., in global model with grid spacing of several kilometers) to deal with gravity waves. This is just when the characteristic method should be used to save computational time and computer resources.

In Fig. 4b, the time series of L_2 and L_∞ are illustrated, as well. Both L_2 and L_∞ increase with time, but are both much smaller in comparison with the results in Fig. 3. At day 12, L_2 and L_∞ display the values of 0.00986 and 0.02751, respectively. They show error increases of 2.4 and 2.6 fold when the time step is increased by three times. As a result, it is possible to enlarge the time step and reduce computational expense in a high-resolution model using the characteristic method. In high-resolution models with grid spacing of several kilometers, the time step restriction due to gravity waves may be only 10 to 20 s in an explicit integration, which is much smaller than the life cycle of cumulus clouds, the variation of solar radiation, and most other modeled physical processes. In both computational and physical senses, the enlargement of the time step becomes a possibility when gravity waves can be treated differently, as here.

To learn about the convergence of the character-

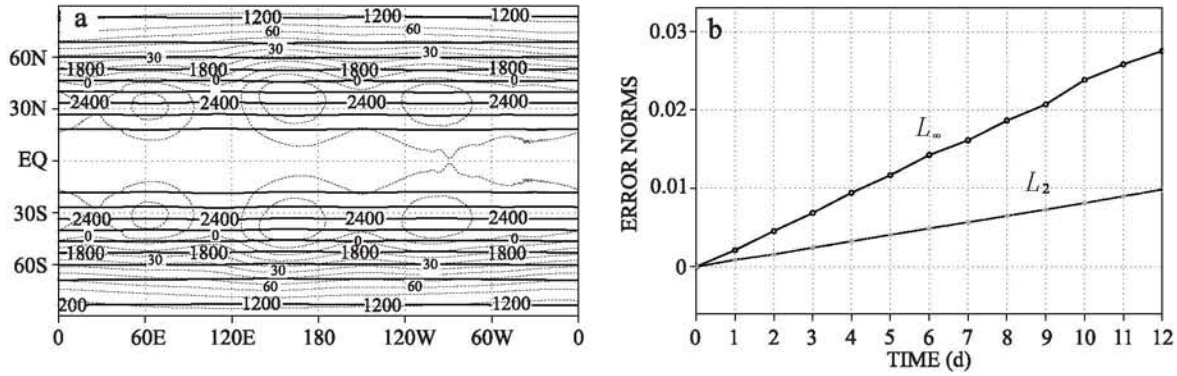

Fig. 4. Numerical results of (a) the geopotential height at day 12 and (b) the corresponding series of error norms, similar to Figs. 2 and 3 except at a resolution of jp=136 with CFL=1.5.

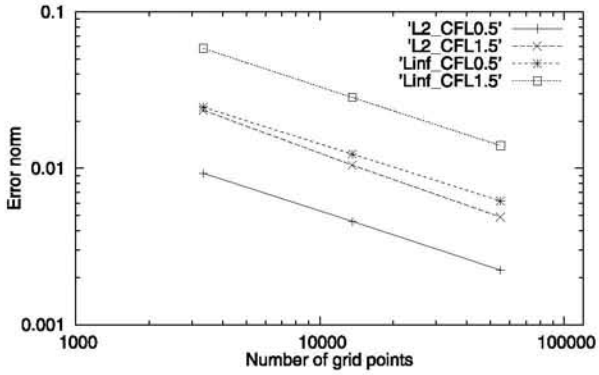

Fig. 5. Variation of the error norms L_2 and L_∞ with grid-point number in the cases of CFL=0.5 and 1.5.

istic method, L_2 and L_∞ variations with grid-point number are shown in log-log coordinates in Fig. 5. The error norms are estimated once per day and averaged over 12 days. They are illustrated with respect to the Courant number cases of 0.5 and 1.5 respectively. Both error norms decline with grid-point number, clearly. In the case of the larger Courant number, a higher convergence rate is displayed because a less conservative reconstruction is performed. As mentioned before, the conservation constraints in this paper only operate at first-order accuracy because the residual of mass is redistributed in accordance with the original mass. The use of large Courant number in a high-resolution model helps to increase the convergence rate with the characteristic method.

5.2 *Solve the zonal flow case over an isolated mountain*

This case is known as Williamson et al. (1992) test 5. The given flow, which is the same as in case 2, impinges on a bell-like mountain. Gravity waves related to the topographic forcing interact with the flow, and these apply stress and result in flow variation. Therefore, the flow is not steady, and no exact solution exists. To evaluate the performance of the characteristic method, we run the shallow water model in a high-resolution configuration ($jp = 130$, $\Delta\lambda = \Delta\varphi = 0.7$) with several Courant number conditions (CFL=0.5, 1.5, and 3.0).

The geopotential height is illustrated with an interval of 5 days in Fig. 6, when the Courant number is fixed at 0.5 or 1.5 (Δt = 105 s or 315 s, respectively). In the case of small time steps, the characteristic method shows similar results as in Li et al. (2008), even though a little rougher spatial distribution is found with the geopotential height in the equatorial zone. Development of a trough in the lee of the bell-shaped mountain displays the proper intensity in comparison with the conservative multi-moment finite-volume shallow-water model (Li et al., 2008) and the spectral method (Jakob et al., 1993). The zonal flow pattern shows a reasonable variation in the computation. Its evolution at high-resolution is confirmed in the small CFL case with the characteristic method.

The variation of the flow pattern and the non-uniform distribution of the wind vector make the computation much difficult in this case, especially for large time steps. In Figs. 6d, 6e, and 6f, the errors increase with time in the integration. Spurious oscillations are mainly observed near the mountain. The trough is greatly deepened in the lee compared with the small time step case. Sharp variations of the vector near topography make the definition of the departure point uncertain. Much more error is therefore observed. The integration, however, is also stable. Low- and high-pressure systems in this test case developed in a quite similar way to the small CFL case.

Further enlargement of the CFL number was also carried out to ensure the stability and accuracy of the characteristic method. When CFL=3.0, stable computation is also achieved, and a similar distribution of the geopotential height is shown at each day of the integration (figure omitted). Due to the large tracking distance for the departure point and the non-uniform wind and height results, the contours display a zigzag pattern in this test. This is shown to be a grid-scale perturbation, which is related to the large difference in departure points for neighboring cell grids. These experiments verifiy the efficiency of the characteristic method in dealing with the gravity wave solution. In practice, the noise may increase with time step enlargement, and no overly large Courant number should be used with a non-uniform flow pattern.

It is worthy noticing that the characteristic method simulates a zonal flow over an isolated mountain very well at low resolution ($jp = 34$, not shown here) with a small time step. However, it fails to simulate the solution properly in the CFL=1.5 case. It suggests that the usage of a characteristic method to enlarge the time step should be limited to high-resolution models. Only in high-resolution cases do numerical models call for large time step.

Using the proposed characteristic method, we successfully simulated cases of a steady geostrophic flow and of zonal flow over an isolated mountain, with gravity waves are treated explicitly. Integration with a large time step is confirmed to be possible in the test cases, and with no matrix inversion needed in the computational procedure. This shows the potential to save computer resources in high-resolution numerical models. This is also the main objective for development of this scheme on a sphere. The conservative properties of the solutions, however, must also be taken into

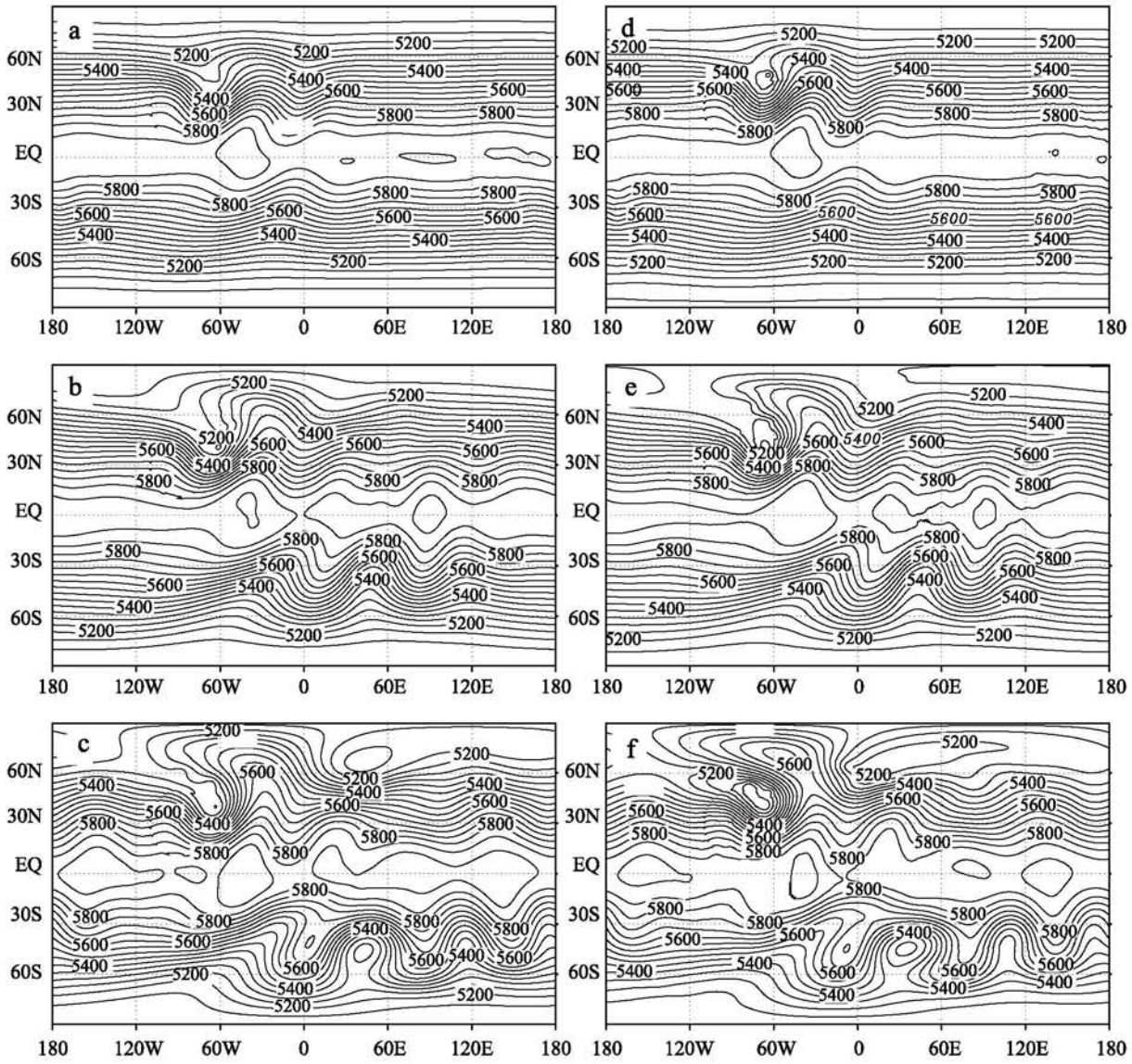

Fig. 6. Evolution of the geopotential height under cases of CFL=0.5 (left) and 1.5 (right) at days 5 (upper), 10 (middle), and 15 (lower) in Williamson et al. (1992)'s test case 5.

account in an assessment of the computational accuracy. The proposed characteristic method based on the advection-form equations, does not ensure conservation, which is a notable shortcoming of the present method in practical computations.

Recently, Chen and Xiao (2008) and Toda et al. (2009) have demonstrated a conservative approach to the Riemann invariant technique, and good numerical results were achieved in cubed-sphere grid and Cartesian grid coordinates, respectively. The conservative characteristic CIP method on a sphere is also being developed on the Yin-Yang grid system with local/global conservative constraints (Peng et al., 2006). It is expected to improve the accuracy of the scheme on the overlapping grid while retaining the intrinsic nature of the present numerical method with respect to not only the efficiency of the integration due to enlargement of the time step, but also by avoidance of matrix inversions.

6. Concluding remarks

By adopting the dimensional splitting CIP algorithm, we have herein proposed the use of the characteristic method to deal with gravity waves explicitly in spherical coordinates. After proper arrangement of terms, the shallow-water model can be solved as an advection equation on sphere. Semi-implicit computation of the Coriolis term and topography-related terms allows integration of the shallow water equation that

is free of CFL limitations. In the semi-implicit semi-Lagrangian integration of the shallow-water model, no matrix inversion appears. This makes the scheme quite economical in a high-resolution model in comparison with the conventional semi-implicit computation of gravity terms.

Computation of the shallow water model solutions for a steady geostrophic flow case and a case of zonal flow over an isolated bell-shaped mountain were carried out, using stable integrations with the proposed scheme, under conditions of large Courant number. The numerical results show the valuable application of the characteristic method to deal with rapid gravity waves in a high-resolution model. Both test cases illustrate that the integration is reasonable and accurate even when computing with CFL=1.5 in a high-resolution configuration.

In the application of this scheme, we also observed that conservation is critical for accurate computation. In the test cases, the global conservation is constrained by redistribution of the residual mass at every time step, because no flux-form dynamical equation is used. The present scheme should be improved to ensure global and/or local conservation, to achieve better accuracy and performance and improve the application to numerical models.

Acknowledgements. The authors are grateful to Prof. Takashi Yabe at Tokyo Institute of Technology for his valuable comments and kind suggestions to improve this work. Thank also Dr. Keiko Takahashi for the useful discussion. The authors appreciate the review and valuable comments given by three anonymous referees. This study is supported by National Natural Science Foundation of China (NSFC) projects (Grant Nos. 40875065 and 40805045), and partially by the research projects 2008R001 at Chinese Academy of Meteorological Sciences (CAMS) and 2008LASWZI05 at the State Key Laboratory of Severe Weather, CAMS.

REFERENCES

Chen, C., and F. Xiao, 2008: Shallow water model on cubed-sphere by multi-moment finite volume method. *J. Comput. Phys.*, **227**, 5019–5044.

Crowley, W. P., 1968: Numerical advection experiments. *Mon. Wea. Rev.*, **96**, 1–11.

Gill, S., 1951: A process for the step-by-step integration of differential equations in an automatic digital computing machine. *Proc. Cambridge Philosophical Society*, **47**, 96–108.

Jakob, R., J. J. Hack, and D. L. Williamson, 1993: Solutions to the shallow water test set using spectral transform method. NCAR Tech. Note NCAR/TN-388+STR, National Center for Atmospheric Research, Boulder, CO, 82pp.

Kageyama, A., and T. Sato, 2004: The "Yin-Yang grid": An overset grid in spherical geometry. *Geochemistry Geophysics Geosystems*, **5**(9), Q09005, doi: 10.1029/2004GC000734.

Li, X., D. Chen, X. Peng, K. Takahashi, and F. Xiao, 2008: A multimoment finite-volume shallow-water model on the Yin-Yang overset spherical grid. *Mon. Wea. Rev.*, **136**, 3066–3086.

McGregor, J. L., 1996: Semi-Lagrangian advection on conformal-cubic grids. *Mon. Wea. Rev.*, **124**, 1311–1322.

Morinishi, Y., O. V. Vasilyev, and T. Ogi, 2004: Fully conservative finite difference scheme in the cylindrical coordinates for incompressible flow simulation. *J. Comp. Phys.*, **197**, 686–710.

Ogata, Y., and T. Yabe, 2004: Multi-dimensional semi-Lagrangian characteristic approach to the shallow water equations by CIP method. *International Journal of Computational Engineering Science*, **5**, 699–730.

Peng, X., F. Xiao, T. Yabe, and K. Tani, 2003: Implementation of the CIP as the advection solver in the MM5. *Mon. Wea. Rev.*, **131**, 1256–1271.

Peng, X., F. Xiao, W. Ohfuchi, and H. Fuchigami, 2005: Conservative semi-Lagrangian transport on a sphere and the impact on vapor advection in an atmospheric general circulation model. *Mon. Wea. Rev.*, **133**, 504–520.

Peng, X., F. Xiao, and K. Takahashi, 2006: Conservative constraint for a quasi-uniform overset grid on sphere. *Quart. J. Roy. Meteor. Soc.*, **132**, 979–996.

Rančić, M. R., J. Purser, and F. Mesinger, 1996: A global shallow-water model using an expanded spherical cube: Gnomonic versus conformal coordinates. *Quart. J. Roy. Meteor. Soc.*, **122**, 959–982.

Rusanov, V. V., 1963: Characteristics of the general equations of gasdynamics. *Zhurnal Vychislitelnoi Mathematiki Mathematicheskoi Fiziki*, **3**, 508–527.

Staniforth, A., and J. Côté, 1991: Semi-Lagrangian integration scheme for atmospheric model—A review. *Mon. Wea. Rev.*, **119**, 2206–2223.

Toda, K., Y. Ogata, and T. Yabe, 2009: Multi-dimensional conservative semi-Lagrangian method of characteristics CIP for the shallow water equations. *J. Comput. Phys.*, **228**, 4917–4944.

Tremback, C. J., J. Powell, W. R. Cotton, and R. A. Pielke, 1987: The forward-in-time upstream advection scheme: Extension to higher orders. *Mon. Wea. Rev.*, **115**, 540–555.

Williamson, D. L., J. B. Drake, J. J. Hack, R. Jakob, and P. N. Swarztrauber, 1992: A standard test set for numerical approximations to the shallow-water equations in spherical geometry. *J. Comput. Phys.*, **102**, 211–224.

Xiao, F., 2004: Unified formulation for compressible and incompressible flows by using multi-integrated moments I: one-dimensional inviscid compressible flow. *J. Comput. Phys.*, **195**, 629–654.

Xiao, F., T. Yabe, and T. Ito, 1996: Constructing oscillation preventing scheme for advection equation by rational function. *Computer Physics Communications*, **93**, 1–12.

Yabe, T., and T. Aoki, 1991: A universal solver for hyperbolic-equation by cubic-polynomial interpolation. I: one dimensional solver. *Computer Physics Communications*, **66**, 219–232.

Yabe, T., R. Tanaka, and F. Xiao, 2001: An exactly conservative semi-Lagrangian scheme (CIP-CSL) in one-dimension. *Mon. Wea. Rev.*, **129**, 332–344.

Zerroukat, M., N. Wood, and A. Staniforth, 2002: SLICE: A semi-Lagrangian inherently conserving and efficient scheme for transport problems. *Quart. J. Roy. Meteor. Soc.*, **128**, 2801–2820.